

## **CHAPTER THREE**

# **SYNTHESIS OF GOLD NANOPARTICLES BY THE UV-IRRADIATION TECHNIQUE**

### 3.0 INTRODUCTION

Morphological control is a useful tool to engineer optical properties of materials but achieving control is still a challenge. Many research groups have reported the synthesis of metal nanoparticles with various shapes such as tetrahedrons [1,2], cubes [3], irregular-prisms [4], rods [5], stars [6] and hollow spheres [7]. The syntheses of anisotropic particles such as nanorods have also attracted considerable attention, due to their relative ease of preparation and rational control of their aspect ratio, which is primarily responsible for the change in their optical properties. Nanorods have been shown to have two plasmon resonances [8], one due to the transverse oscillation of the electrons around 530 nm for gold and the other due to the longitudinal plasmon resonance at longer wavelengths. The transverse surface plasmon resonance does not depend on the aspect ratio and is at the same wavelength as the plasmon resonance of spheres [8]. However the longitudinal surface plasmon resonance increases with large aspect ratios [8].

Triangular nanoparticles have been produced by photochemical [9] and chemical growth methods [10]. The corners and edges are very important with triangular nanoparticles. Snipping of the edges produces a visible blue shift in the plasmon resonance [9], which can be modelled theoretically [11,12]. Miranda and Ahmadi [13] have studied the growth of gold nanorods by the photochemical reduction of  $\text{HAuCl}_4$  in micelle solutions. They found that the anisotropic growth of gold nanoparticles was intensively affected by the wavelength of UV light source and their photon flux. Yang *et al.* [14] reported that the pH value of the solution played an important role both in the photochemical reduction of Au (III) to  $\text{Au}^0$  and in the formation process of gold nanoparticles under UV-irradiation. Chen *et al.* [15] prepared truncated tetrahedral, cubic and octahedral gold nanoparticles and hexagonal nanosheets by introducing a small amount of salt into a *N,N*-dimethylformamide (DMF) solution containing PVP.

In this chapter the synthesis of anisotropic polymer capped gold nanoparticles using the previously reported UV-irradiation reduction technique is described [14]. In this work polyvinyl alcohol (PVA) and polyvinyl pyrrolidone (PVP) are used as capping ligands.

The effect of polymer and metal salt concentration, lamp power, capping agent, solvent and irradiation time on the nanoparticle morphology were monitored. In a typical preparation procedure, a column like low-pressure mercury lamp was used as an ultraviolet irradiation source. The gold source,  $\text{HAuCl}_4$  and polymer are mixed and dissolved in a solvent prior to the reduction of  $\text{Au}^{3+}$  to  $\text{Au}^0$  by UV-irradiation light from the uv-lamp with wavelength of 450 – 500 nm. The gold salt absorbs the UV-light to generate an excited electronic state, and then reacts with polymer which also serves as the capping agent. The role of these polymers is two-fold, it strongly complexes to the gold ion, and also acts as a capping ligand for the formed gold nanoparticles. Reaction parameters such as the concentration of gold salt and polymer and the irradiation time are important in determining the final shape of the gold nanoparticles. These experiments demonstrate that the UV-irradiation technique is an efficient and versatile approach for the consistent preparation of nanoparticles that exhibit a high degree of purity.

### 3.1 EXPERIMENTAL

#### 3.1.1 Materials and Instrumentation

Water was mostly used as the solvent to generate gold nanoparticles and in some reactions alcohol (ethanol) and acetonitrile were used. The chemicals used in the synthesis were procured from standard suppliers. Hydrogen tetrachloroaurate ( $\text{HAuCl}_4 \cdot 3\text{H}_2\text{O}$ ), PVP, PVA, citric acid were obtained from Aldrich and used as received.

The details of instrumentation are similar to that described in Chapter 2.

#### 3.1.2 Synthesis of Gold Nanoparticles: Variation of Polymer Concentration

In a typical reaction  $\text{HAuCl}_4$  (0.033 g) and PVP (0.400 g) were dissolved in distilled water (200.0 mL) which formed a yellow solution. This solution was then irradiated with a column-like mercury lamp (450 - 500 nm) under nitrogen atmosphere, resulting in a dark wine-red coloured solution. The reaction was irradiated for 24 h to ensure the completion of the process. The particle growth and morphology was monitored with time. This was done by syringing out samples at time intervals from 5 min to 24 h. The

syringed products were centrifuged to remove the ions in the final products. The concentration of the stabilizing agent was varied in order to determine its effect on size and morphology of the gold nanoparticles. In a typical experiment all the other conditions were maintained and PVP concentration was doubled, i.e. 0.800 g. The experiment was repeated by changing the capping agent to PVA.

### **3.1.3 Synthesis of Gold Nanoparticles: Variation of Metal Source Concentration**

The reaction procedure is as described in the previous section **3.1.2** and was repeated with a variation of the concentration of the metal source. The reaction was repeated using metal source ( $\text{HAuCl}_4$ ) amounts of 0.015 g and 0.045 g with irradiation up to 24 h. The effect of the variation of the metal source was also performed when the capping agent was changed to PVA.

### **3.1.4 Synthesis of Gold Nanoparticles: Variation of Lamp Wavelength**

The reaction procedure is as described in section **3.1.2** and was repeated with the varied wavelength of the UV lamp. The lamp settings 400 – 450 nm (wavelength), 6 W and 125 W were used.

### **3.1.5 Synthesis of Gold Nanoparticles: Variation of Solvent**

The reaction procedure is as described in section **3.1.2** and was repeated with solvent changed from water to ethanol and acetonitrile. The effect of the three solvents (water, ethanol and acetonitrile) on the size and shape of gold nanoparticles was studied.

### **3.1.6 Synthesis of Gold Nanoparticles: Polymer and Irradiation Time Variation**

In the typical reaction  $\text{HAuCl}_4$  (0.033 g) and PVP (0.800 g) were dissolved in distilled water (200.0 mL) to form a yellow solution. This solution was then irradiated with a column-like mercury lamp (450 - 500 nm) under nitrogen atmosphere, resulting in a dark wine-red colour solution. The reactants were irradiated for 24 h to ensure the completion of the growth process. The particle growth and morphology were monitored with time. This was done by taking out aliquots at time intervals from 5 min to 24 h. The

syringed products were centrifuged to remove the ions in the final product. The stabilizing agent was varied to PVA under the same reaction conditions. For this reaction, PVA was first dissolved separately in distilled water at 80 °C and brought to room temperature before mixing with the  $\text{HAuCl}_4$  solution. A separate experiment was conducted just to monitor the irradiation time on the size and intensity of prepared gold nanoparticles.

### 3.1.7 Synthesis of Gold Nanoparticles in the Presence of Citric Acid

In the typical reaction  $\text{HAuCl}_4$  (0.050 g), PVP (0.030 g), and citric acid (0.1153 g) were dissolved in distilled water (200.0 mL) which formed a yellow solution. This solution was then irradiated with a column-like mercury lamp (125 W) under nitrogen atmosphere. The reaction mixture was irradiated for 60 min to ensure the completion of the process. This was done by syringing out samples at regular intervals from 8 min to 60 min. The syringed products were centrifuged to remove the unwanted ions from the final products.

All the above synthesis protocols for the production of gold nanoparticles are listed in [Table 3.1](#). [Figure 3.1](#) shows the UV-irradiation technique set-up in the laboratory for the synthesis of shaped-AuNPs. It can be clearly seen that through irradiation the metal is reduced as confirmed by the new colour change to wine red observed from the solution.

**Table 3.1:** Reaction conditions used for the synthesis of gold nanoparticles.

| Exp | HAuCl <sub>4</sub><br>(g) | Stabilizer |            | Lamp<br>(wavelength /<br>Watts) | Solvent       |                 |                      |
|-----|---------------------------|------------|------------|---------------------------------|---------------|-----------------|----------------------|
|     |                           | PVP<br>(g) | PVA<br>(g) |                                 | Water<br>(mL) | Ethanol<br>(mL) | Acetonitrile<br>(mL) |
| 1   | 0.033                     | 0.400      | —          | 450 – 500 nm                    | 200           | —               | —                    |
| 2   | 1.000                     | 0.400      | —          | 400 – 450 nm                    | 200           | —               | —                    |
| 3   | 0.033                     | 0.800      | —          | 400 – 450 nm                    | 200           | —               | —                    |
| 4   | 0.033                     | —          | 0.400      | 450 – 500 nm                    | 200           | —               | —                    |
|     | 0.033                     | —          | 0.800      | 450 – 500 nm                    | 200           | —               | —                    |
| 5   | 0.300                     | —          | 0.400      | 450 – 500 nm                    | 200           | —               | —                    |
|     | 0.300                     | —          | 0.800      | 450 – 500 nm                    | 200           | —               | —                    |
| 6   | 0.015                     | 0.750      | —          | 125 Watts                       | 200           | —               | —                    |
| 7   | 0.045                     | 0.750      | —          | 125 Watts                       | 200           | —               | —                    |
| 8 * | 0.050                     | 0.030      | —          | 125 Watts                       | 200           | —               | —                    |
| 9   | 0.033                     | 0.400      | —          | 125 Watts                       | 200           | —               | —                    |
| 10  | 0.033                     | 1.200      | —          | 125 Watts                       | 200           | —               | —                    |
| 11  | 0.033                     | 0.400      | —          | 125 Watts                       | —             | 200             | —                    |
| 12  | 0.033                     | 0.400      | —          | 125 Watts                       | —             | —               | 200                  |
| 13  | 0.033                     | 0.099      | —          | 125 Watts                       | 200           | —               | —                    |

\* 0.1153 g of citric acid was added.

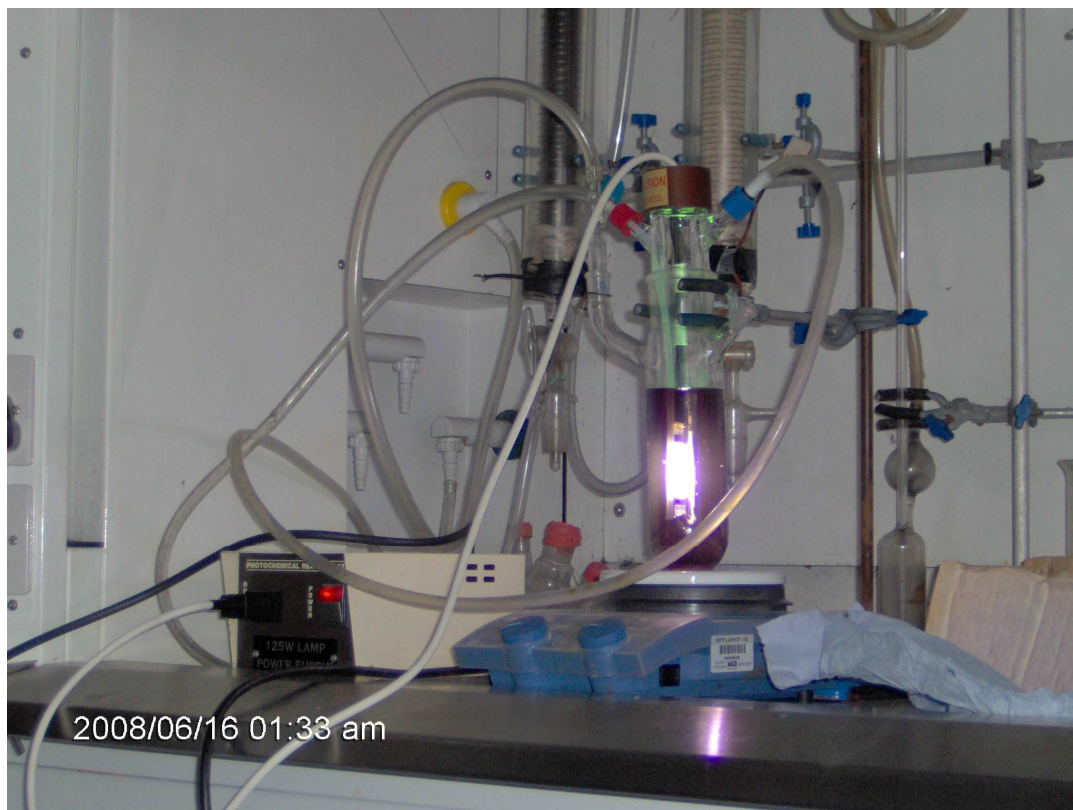


**Figure 3.1:** Setup for the synthesis of AuNPs via the UV-irradiation technique.

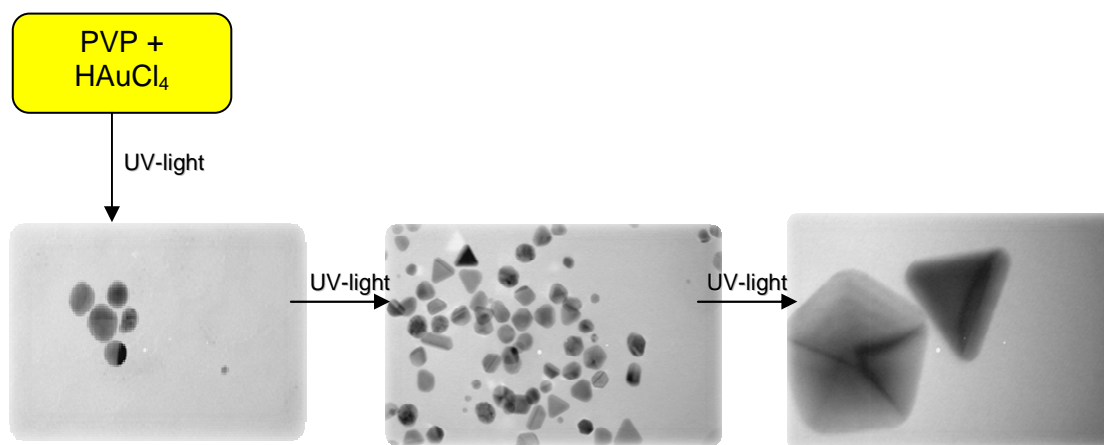


**Figure 3.2:** Pathway of photochemical formation of the precursor solution into shaped AuNPs monitored by TEM.

## 3.2 RESULTS AND DISCUSSION

AuNPs have been synthesized by the photochemical transformation of a precursor solution to gold nanoparticles. The solution was produced by dissolving salt ( $\text{HAuCl}_4$ ) and PVP, a stabilizing agent, in distilled water. The metal was then reduced by UV-light to form AuNPs of different shapes. Upon reduction, a yellow solution turned to light wine-red consisting of small spherical AuNPs. Upon exposure to intense visible light from a mercury lamp, the precursor solution became purple or intense wine-red. At this stage it comprised of large particles with varying shapes. Upon further exposure, the solution display deep wine-red colour with the presence of larger 3-D nanoparticles. These larger non-spherical AuNPs comprise amongst them, triangular, truncated triangular, hexagon, pentagon and decahedra shaped nanoparticles. The multiple-AuNPs formation through the transformation of the yellow precursor solution is schematically shown in [Figure 3.2](#). Light exposure is essential for the multiple-shaped formation; the precursor solution does not form nanoparticles at a minimum and low light exposure.

### 3.2.1 Variation of Polymer Concentration (PVP)

The optical properties of as prepared AuNPs were investigated by UV-Visible absorption spectroscopy as shown in [Figure 3.3A](#) and [B](#). The absorption spectra shown in this figure are for AuNPs synthesized at conditions of experiment 1 as outlined in [Table 3.1](#). The light yellowish colour of the aqueous  $\text{HAuCl}_4$  solution exhibits an intense absorption band at 292 nm because of metal-ligand charge transfer (MLCT) band from the  $\text{AuCl}_4^-$  complex [[16](#)]. The absorption spectra of all samples shows a broad band with the peak at around 530 nm, present in all the spectra and is, attributed to the transverse surface plasmon resonance (SPR) mode of spherical AuNPs [[15](#)]. An additional low intensity absorption peak at a longer wavelength (720 – 900 nm) was also observed which is due to the longitudinal SPR. It can be inferred from the absorption spectra that all samples consist of a mixture of diverse shaped nanoparticles. The effect of the stabilizing agent (PVP) on the size and morphology of AuNPs was also studied. In the conditions of experiment 10 in [Table 3.1](#), the PVP concentration was tripled. UV-Visible spectroscopy was used for optical characterization as shown in [Figure 3.3B](#).

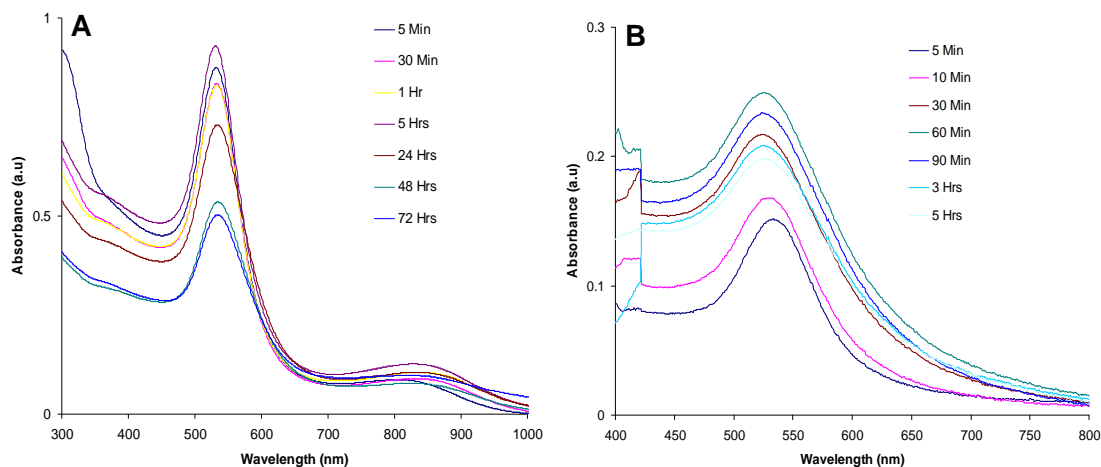


**Figure 3.3:** UV-Visible absorption spectra of AuNPs at various PVP concentrations and various irradiation times; **A.** 0.4 g PVP, and **B.** 1.2 g PVP.

In this experiment the solution was exposed to light for 5 h. At high PVP concentration, no secondary absorption was observed as is the case with experiment 1 results. The AuNPs prepared both at low and high stabilizing agent concentrations were characterized by TEM for their structural properties. The TEM images of the purified samples at low PVP concentration confirm the diversity of particle shapes. TEM micrographs at 5 minutes irradiation time shows particles which were predominantly spherical in shape with some low percentage of faceted nanoparticles as shown in [Figure 3.4A](#). Pentagonal, hexagonal, truncated triangular and rod-shaped nanoparticles are observed at different irradiation times of the precursor solution.

There were previous reports of hexagonal shaped AuNPs in PVP; however the anisotropic shape had to be induced by the addition of a salt [14]. The UV-irradiation method has also produced hexagonal shaped nanoplates in the presence of citric acid. Yang *et al.* [17] synthesized gold nanoparticles with varying morphologies by a continuous method under UV-irradiation in the presence of citric acid and PVP. The shape of the particles was determined by experimental parameters such as PVP concentration and flow rates. However triangular and hexagonal shaped particles were only obtained in the absence of PVP and a low solution flow rate. In this work as the irradiation time was increased to 30 minutes, more distinct non-spherical nanoparticles in the form of decahedrons and hexagons were observed ([Figure 3.4B](#)). The decahedron is a

basic multiply twinned structure which consists of five tetrahedral crystallites with bare {111} surfaces [17]. Shape evolution was further detected after 5 and 24 hours of irradiation time, truncated triangular gold particles were observed in addition to the more distinct hexagonal and decahedral shaped particles (Figures 3.4C and D). The presence of longer rod shaped particles is also observed. A further exposure to light for 48 and 72 hours resulted in well-dispersed truncated triangular-shaped nanoparticles while at longer times of irradiation clustered nanoparticles are observed; pointing to saturation of the reaction (Figures 3.4E and F).

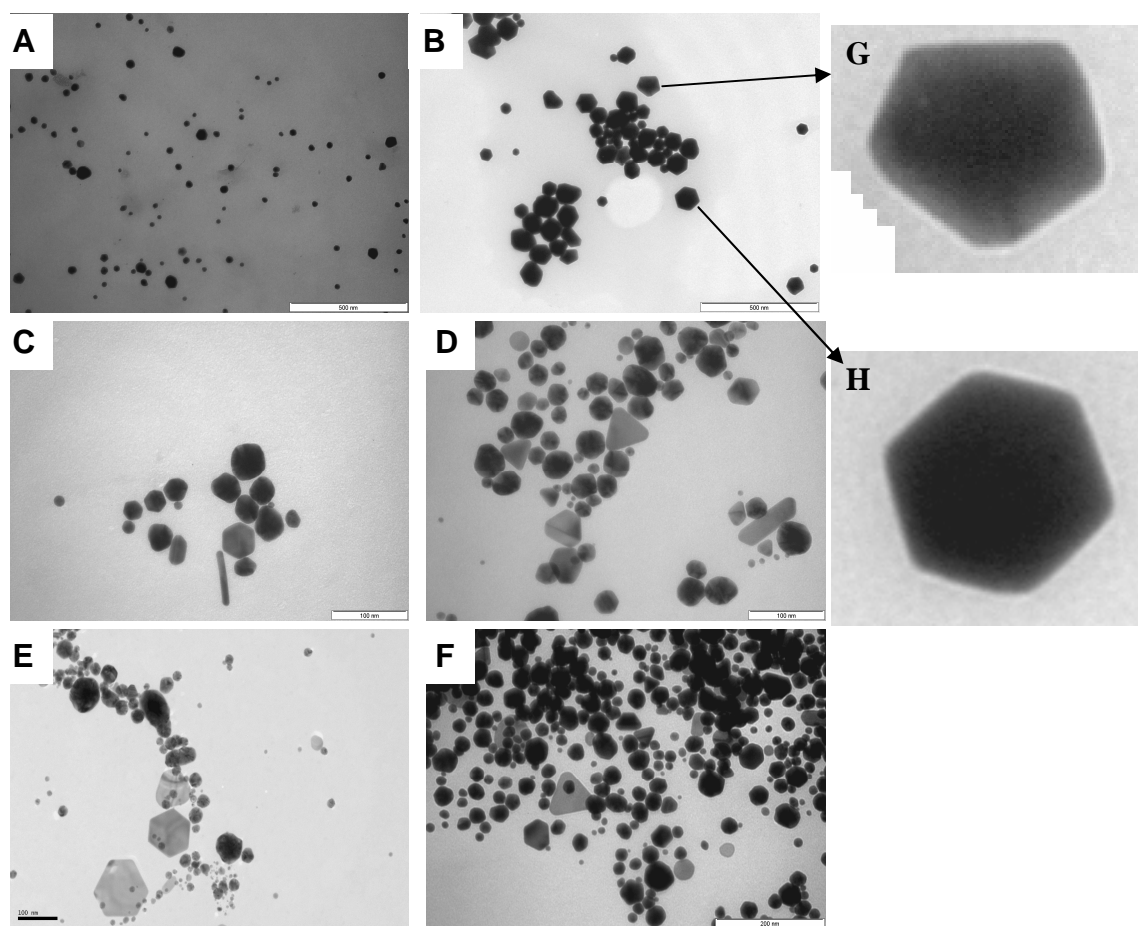


**Figure 3.4:** TEM images of AuNPs at low PVP concentrations synthesized after A. 5 min B. 30 min, C. 5 hours, D. 24 hours, E. 48 hours and F. 72 hours, G. and H. are at high magnification.

A detailed explanation for the formation of gold nanoparticles in the form of hexagons, decahedrons and truncated triangles by UV-irradiation in the presence of PVP is not very clear. Previous reports on gold and silver nanoplates suggest that the shape of the particles depend upon the selective adsorption of PVP on the surface of the particles [18]. The PVP plays an important role in controlling the growth rate between the {100} and {111} plane directions by altering their surface energies [1,19,20]. In this case as the gold salt is reduced under UV-irradiation there is adsorption of the PVP on the newly formed gold particles. The variety of particle shapes formed at various irradiation times is probably due to the effect of the ratio of the reduced gold to PVP as the reaction proceeds. The decrease in concentration of PVP as the irradiation time increases has an influence on the surface free energies of the various crystal planes thereby resulting in varying morphologies. At certain stages adsorption along the {111} surface is probably favored due to its low surface free energy resulting in the formation of {111} facets and decahedral multiply-twinned particles (MTPs).

TEM micrographs for AuNPs at high concentration of the stabilizing agent, PVP, were not different from one another (Figure 3.5). Most spherical particles were observed at 5 min of irradiation. At 30 min, differently shaped (irregular) particles were observed including triangular and decahedron shaped particles, with particles having sizes ranging between 5 - 20 nm. From 1 hour up to 24 hours of irradiation nanoparticles formed were dense and cloudy from the micrographs which clearly indicate the excess of the capping agent. Figure 3.6 shows the high resolution TEM micrograph for AuNPs synthesized at a low stabilizing agent concentration as well as the X-ray powder diffraction showing the crystallographic properties for both low and high PVP concentrations. The HRTEM image clearly shows lattice fringes of gold and confirms the crystallinity of such materials.

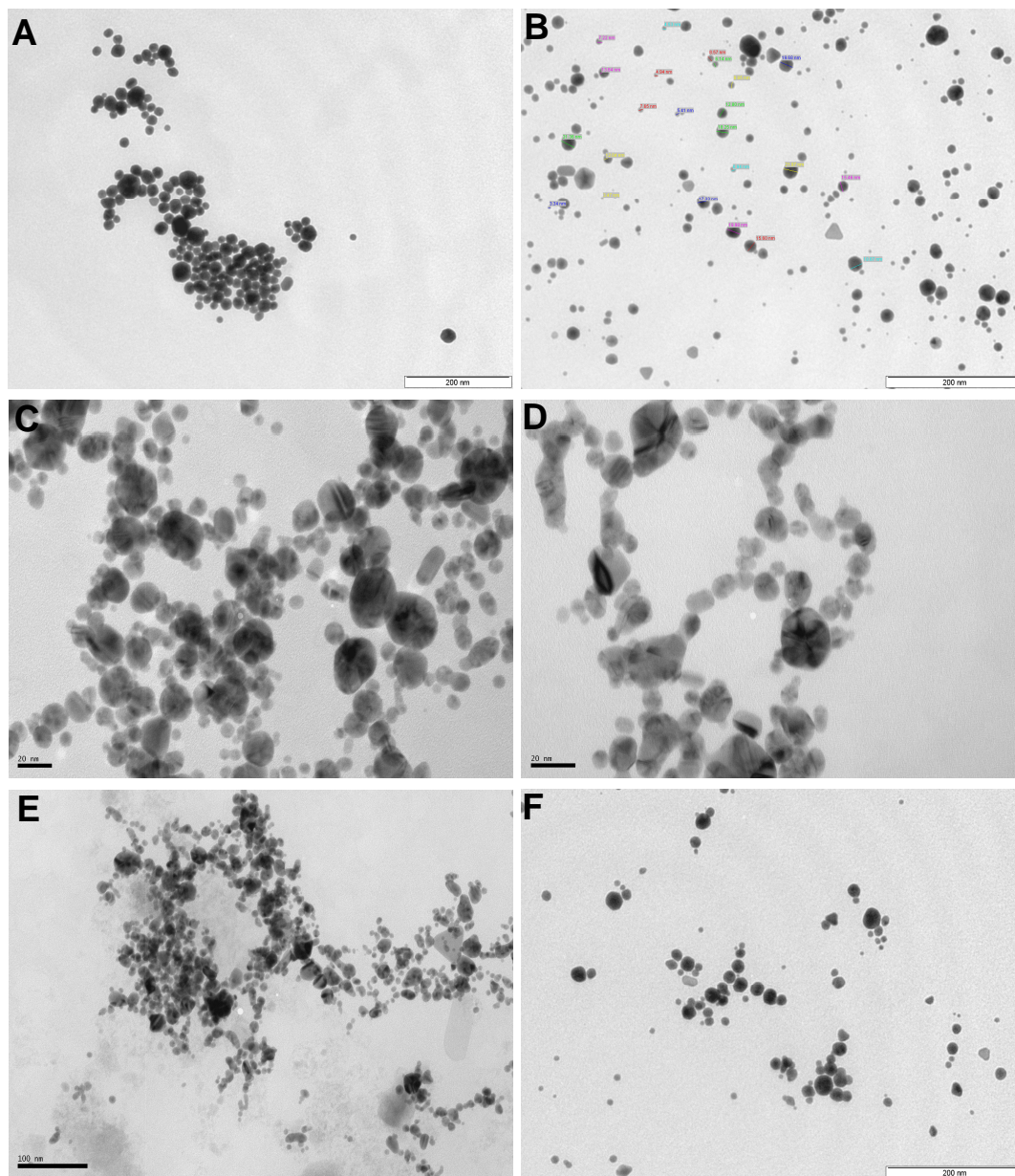


**Figure 3.5:** TEM images of AuNPs at high PVP concentrations synthesized after A. 5 min, B. 30 min, C. 1 hour, D. and E. 3 hours and F. 24 hours.

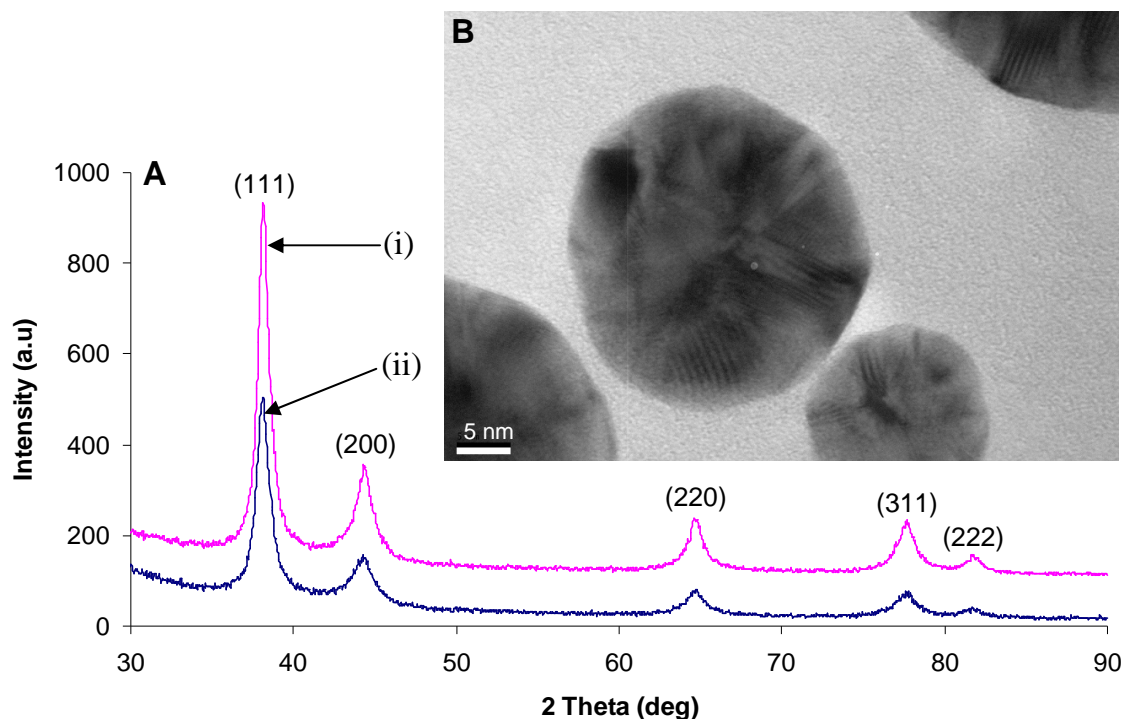


**Figure 3.6:** A. XRD pattern for AuNPs at low and high PVP concentration (i) 0.4 g and (ii) 1.2 g; B. High magnification of AuNPs at low PVP concentration.

All diffraction peaks observed from the XRD data were indexed to the characteristic peaks of AuNPs. The Bragg reflection obtained from the AuNPs clearly corresponds to the fcc crystalline structure of gold [21]. The peaks are assigned to the diffraction from (111), (200), (220), (311) and (222) planes of fcc gold respectively. (JCPDS File 04-0784).

### 3.2.2 Variation of Polymer (PVA) Concentration

Figure 3.7 shows the characterization of AuNPs synthesized as outlined in experiment 5, Table 3.1. The UV-Visible spectrum for the particles synthesized at high PVA concentration shows absorption at 533 nm which is blue shifted from that of low PVA concentration particles which absorb at 570 nm. Broadening of the spectrum at longer wavelengths is observed for the high PVA concentration experiment, an indication of the presence of non-spherical AuNPs.

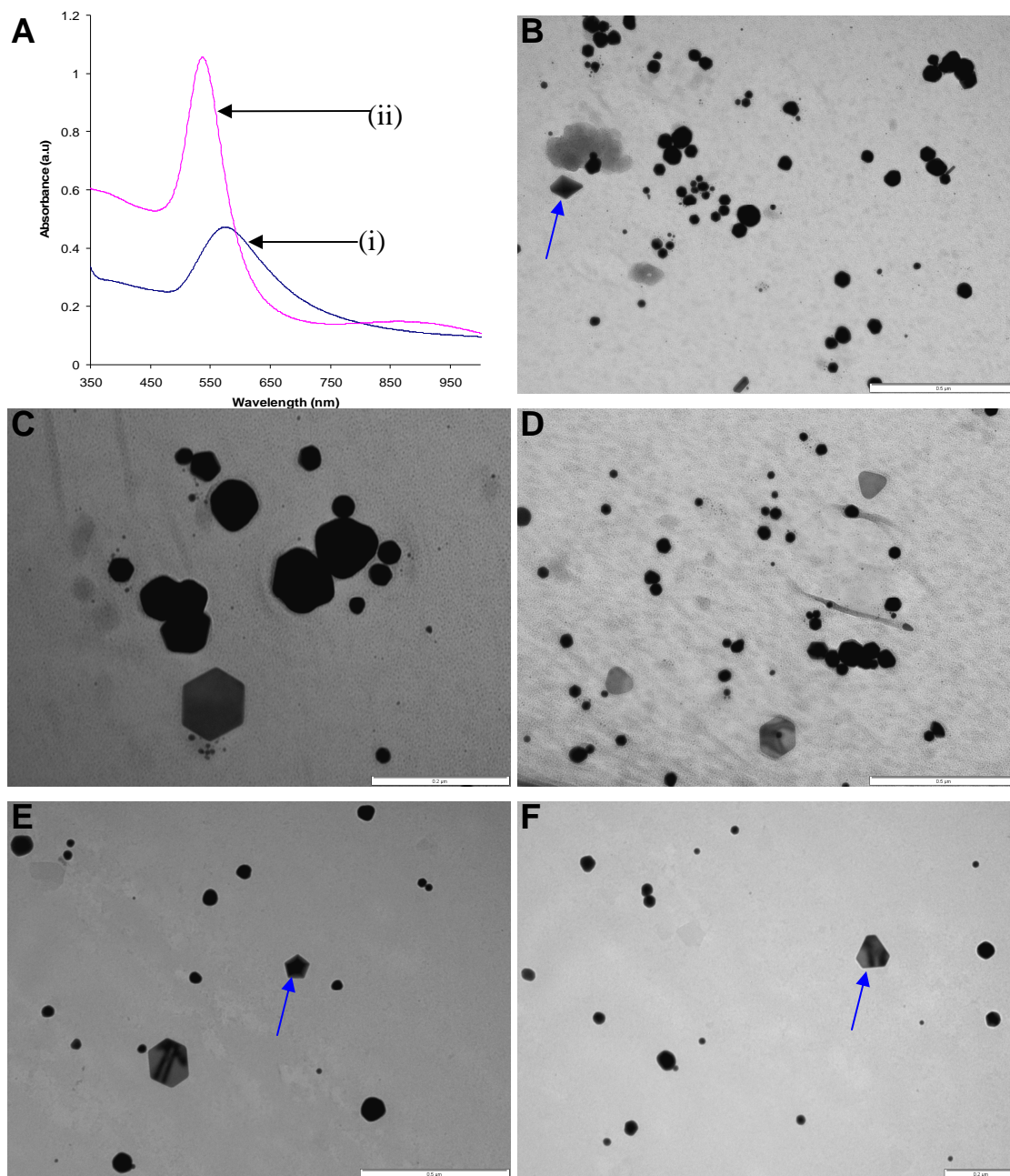


**Figure 3.7:** A. UV-Visible absorption spectra of AuNPs at various PVA concentrations; (i) 0.400 g and (ii) 0.800 g, (B – D) TEM images of AuNPs at low PVA concentration, (E and F) TEM images of AuNPs at high PVA concentration.

The morphological analysis for both the low (images B-D) and high (images E and F) PVA concentration indicates the presence of anisotropic nanoparticles, some of which are

clearly shown in the [Figure 3.7](#). Also common in these micrographs is the good dispersity and low yield of nanoparticles.

### 3.2.3 Variation of Metal Source Concentration

The AuNPs were synthesized by the photochemical reduction at different concentrations of the gold salt,  $\text{HAuCl}_4$ . The results of the experiments 6 and 7 from [Table 3.1](#) are discussed in this section. The effect of the irradiation time on the solutions with different precursor concentrations was studied by UV-Vis spectroscopy as shown in [Figure 3.8](#). The figure shows the absorption as a function of wavelength for both the low and high precursor concentration at different irradiation time. The SPR absorption at 530 nm is monitored as a function of reaction time. The exposure of the precursor solution to light was stopped at maximum irradiation time and the solution was left at room temperature. The absorbance of the generated AuNPs is found to increase as irradiation time is increased. The increase in time also resulted in a blue-shift in the absorption spectra from that at least irradiation time, i.e. 5 minutes. At the end of irradiation there is no absorption peak due to  $\text{Au}^{3+}$  which confirms its complete reduction in the solution.

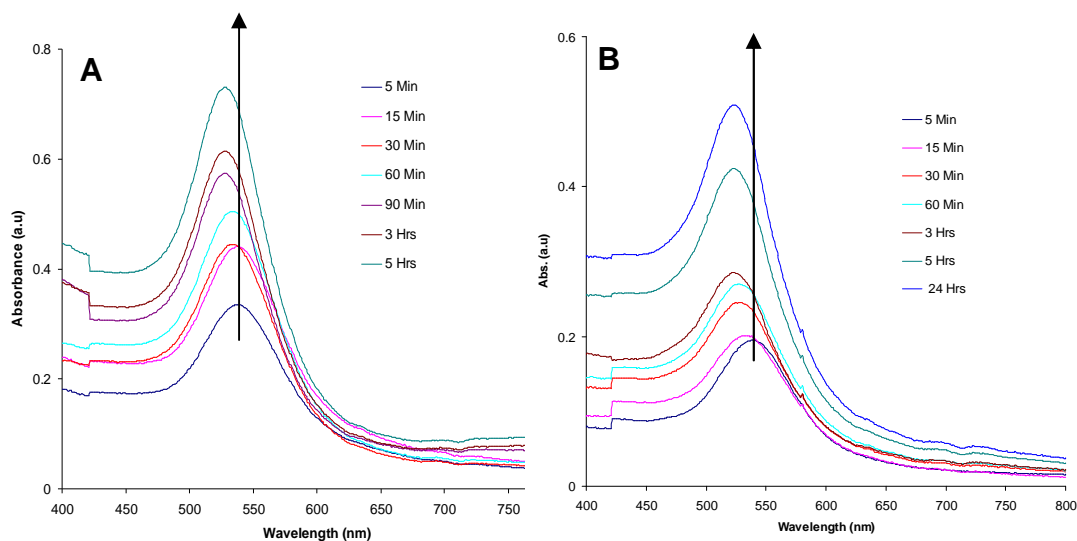


**Figure 3.8:** UV-Visible absorption spectra of AuNPs at various  $\text{HAuCl}_4$  concentrations and various irradiation times **A.** 0.015 g  $\text{HAuCl}_4$  and **B.** 0.045 g  $\text{HAuCl}_4$ .

TEM was used for the structural and morphological analyses on the samples that were taken at maximum irradiation time in both the experiments. Figure 3.9 represents TEM images for the AuNPs solution having the low concentration of the precursor (0.015 g of  $\text{HAuCl}_4$ ) and at longest irradiation time i.e. 5 hours. This showed that the sample contained above 90 % of non-spherical AuNPs, with average size in the nanometer range. The particles were well dispersed throughout different parts of the copper grid. Triangular, truncated triangular, pentagon, hexagon, nanoprisms, rods, octahedral and decahedra shaped nanoparticles are observed at different magnifications.

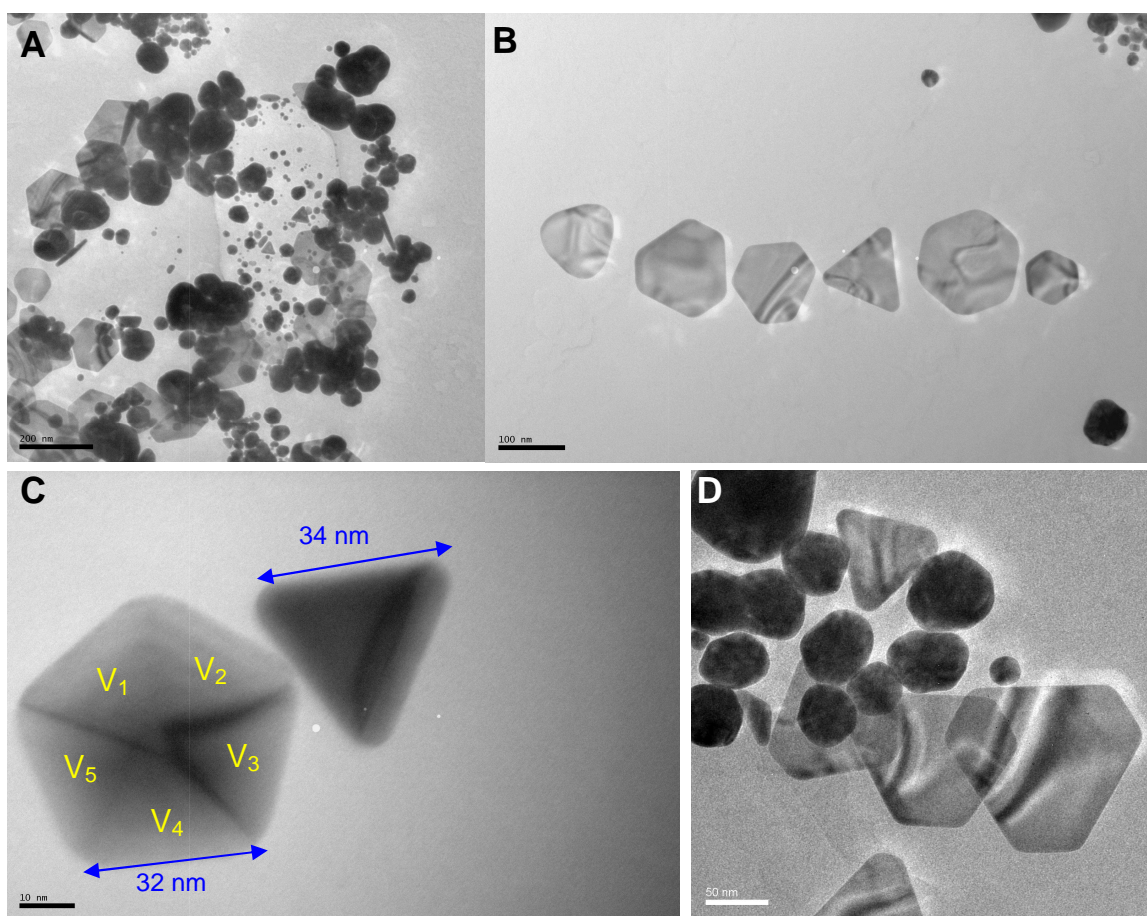


**Figure 3.9:** TEM images of AuNPs at low precursor concentration (0.015 g of  $\text{HAuCl}_4$ ) for the sample taken at longest irradiation time (5 hours). Images A, B, C, and D are at different magnifications and different parts of the copper grid.

It is known that lowering the precursor concentration reduces the chemical potential for crystallization [22]. It has also been theoretically demonstrated that the small sizes

five-fold multiply twinned icosahedra and decahedra structures are the most thermodynamically stable seed, as it is bound almost entirely by the lower energy {111} facets [23,24]. Thus, by lowering the precursor concentration it is possible to decrease the chemical potential to a sufficiently low level so that multiple-twinned particles (MTPs, thermodynamically more stable, often in the decahedral shape) rather than single-crystal seeds (kinetically stable) will be formed. Figure 3.9C shows a nanoprism with side that are 34 nm long and a decahedral shaped nanoparticles which have a pentagonal cross section, 32 nm long sides. This pentagonal cross section clearly discloses the five-fold contrast resulting from the differences in crystal orientation induced by the twin defects. The stark contrast across each twin plan implies that each gold nanowire contained five single-crystal units, which are marked as  $V_1$ ,  $V_2$ ,  $V_3$ ,  $V_4$ , and  $V_5$ . Figure 3.9D showed the presence of truncated triangular shaped nanoparticles with short and long sides lying on top of each other. The growth is taking place along these short edges as a result of shape evolution into a normal triangular shaped particle [23].

The HRTEM and selected area electron diffraction (SAED) for AuNPs prepared both at low and high precursor concentrations are also reported. Figure 3.10 gives a clear evidence of the crystallinity in nanoparticles prepared in each of these experiments. In Figure 3.10A and B lattice fringes are clearly seen, while in image C spherical and penta-twinned particles are observed. The lattice spacing of 1.5 nm corresponds to the (220) plane of fcc gold. Figure 3.10D represents the SAED pattern taken at single nanocrystal of AuNP. The clearly defined diffraction rings confirms the crystallinity of the particles.

TEM images of AuNPs solution having the high concentration of the precursor (0.045 g) is also reported for samples at longest irradiation time. Figure 3.11 presents these micrographs at different magnifications and parts of the copper grid. Multiple shaped AuNPs are observed in these micrographs with size ranging from 25 - 50 nm. This showed a high yield of nanoparticles which are well distributed on the copper grid. The crystalline nature of the particles was also observed from the HRTEM and SAED for the gold particles synthesized at a high precursor concentration as seen in Figure 3.12.

Particles in the shape of a triangle and multiply twin structure are observed. The SAED pattern indicates that the particles are crystalline.

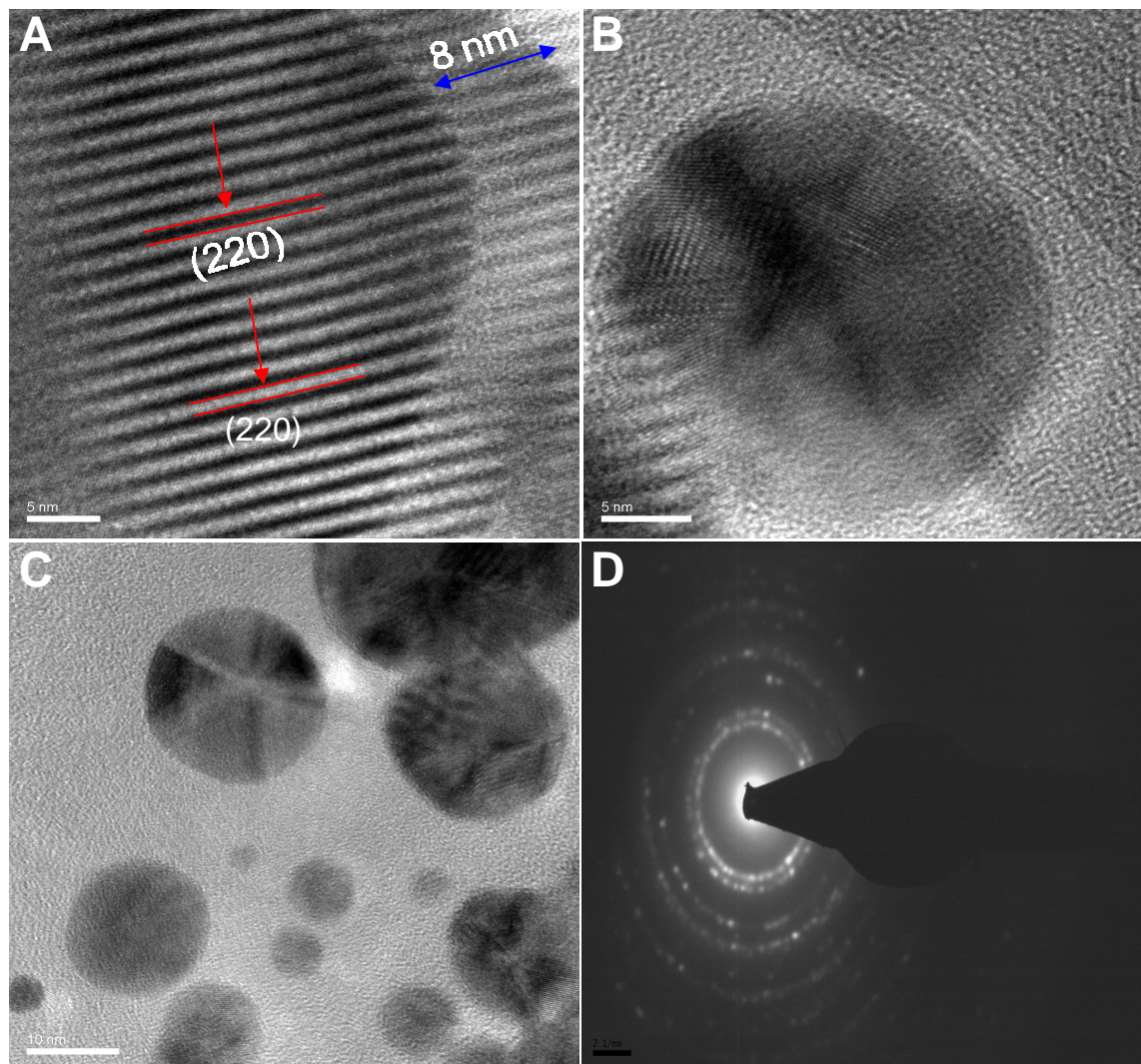


**Figure 3.10:** A, B and C are HRTEM micrographs of AuNPs at low precursor concentration (0.015 g of  $\text{HAuCl}_4$ ) for the sample taken at longest irradiation time (5 hours), image D is the SAED pattern.

Figure 3.13 presents the results obtained from the XRD analysis. All the diffraction peaks observed can be indexed to the characteristics of AuNPs. The peaks are assigned to the diffraction from the (111), (200), (220), (311) and (222) planes of fcc gold respectively (JCPDS File 04-0784).

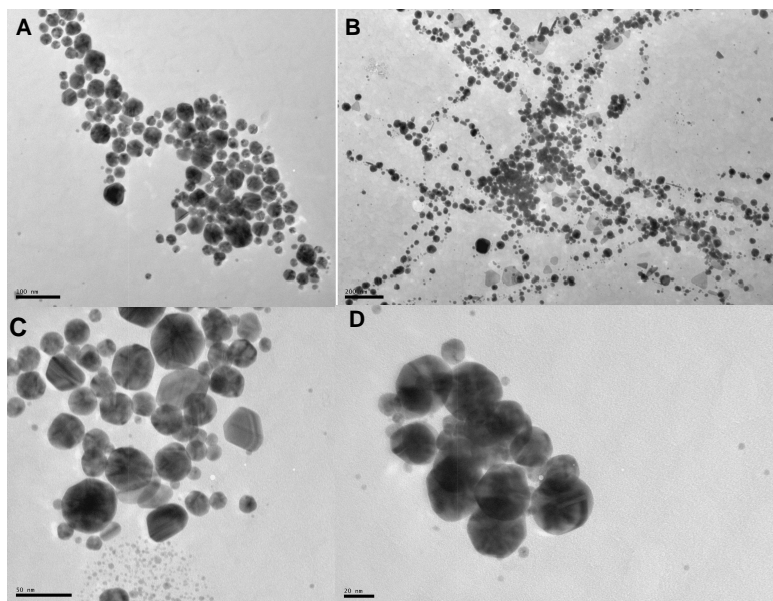


**Figure 3.11:** TEM images of AuNPs at high precursor concentration (0.045 g of  $\text{HAuCl}_4$ ) for the sample at longest irradiation time (5 hours). Images A, B, C and D are at different magnifications and different parts of the copper grid.

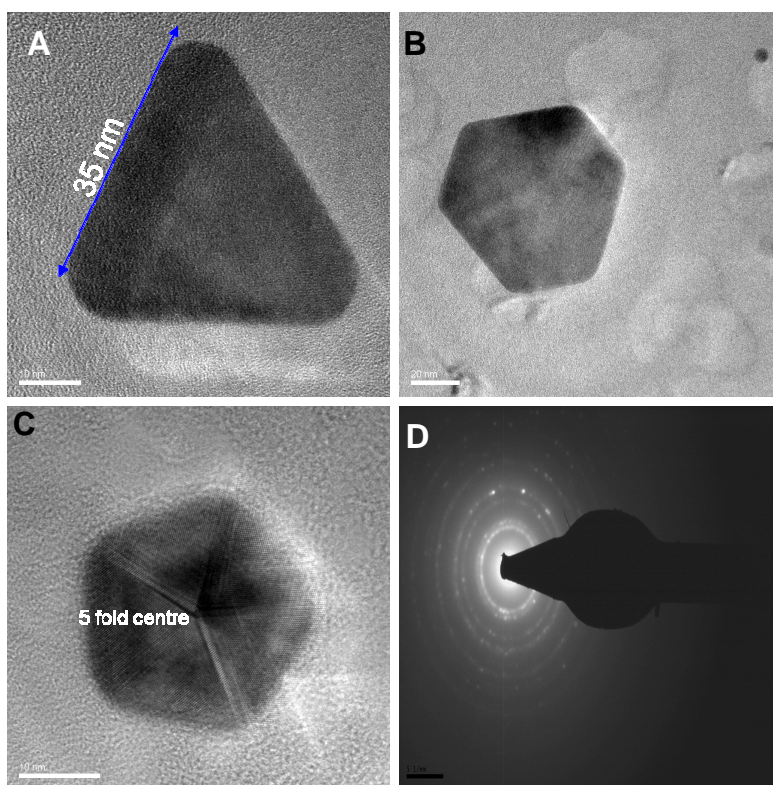


**Figure 3.12:** A, B and C are HRTEM images of AuNPs at high precursor concentration (0.045 g of  $\text{HAuCl}_4$ ) for the sample taken at longest irradiation time (5 hours), Image D is the SAED pattern.

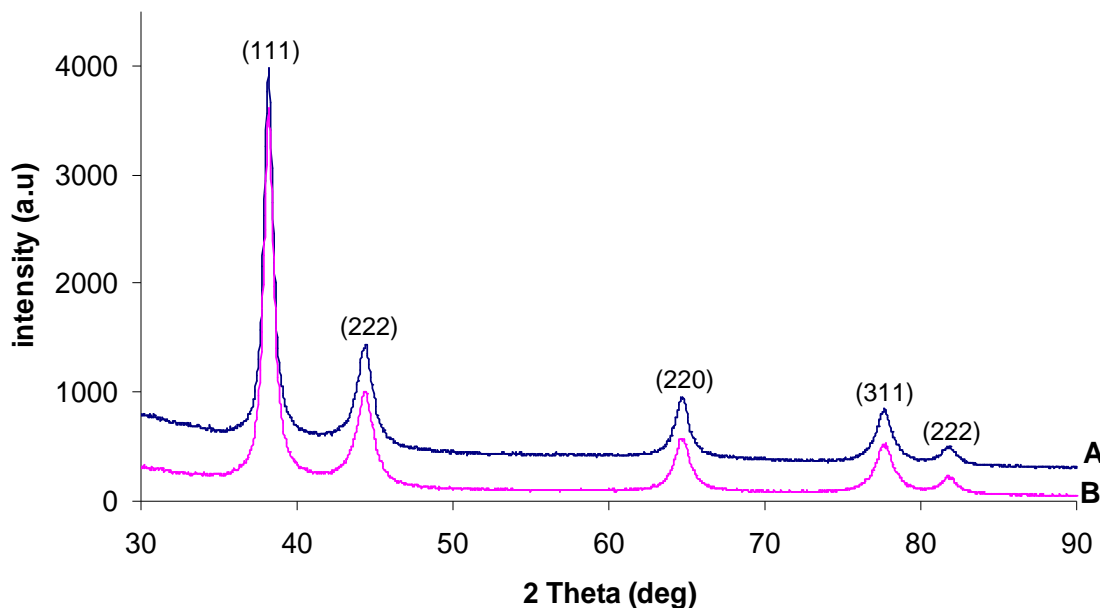


**Figure 3.13:** Powder XRD pattern of the AuNPs, (A) low precursor concentration (0.015 g HAuCl<sub>4</sub>) and (B) high precursor concentration (0.045 g of HAuCl<sub>4</sub>).

### 3.2.4 Variation of the Solvent

The results reported in this section are for the experiments 9, 10 and 11 as outlined in Table 3.1. The solvent in which the AuNPs are synthesized has been varied. The SPR absorption band appeared at around 520 nm with an increase in intensity as a function of irradiation time. A similar change in the absorption spectrum was also observed for AuNPs produced in other organic solvents, except that at the lowest irradiation times no absorption was observed and the absorption band is red-shifted from that of aqueous solution with increasing UV-irradiation time. Figure 3.14 shows the absorption spectra at shortest and longest irradiation times for AuNPs in three different solvents, i.e. water, ethanol and acetonitrile. There is no absorption for acetonitrile at 5 minutes while ethanol at the same time shows the presence of absorption. AuNPs are produced in water after 5 minutes of irradiation with a broad peak observed around 550 nm. As the irradiation time was elevated to 5 hours, the two organic solvents showed absorption peaks that were red-shifted from that of water (527 nm), with acetonitrile having a peak at 537 nm and ethanol at 535 nm.

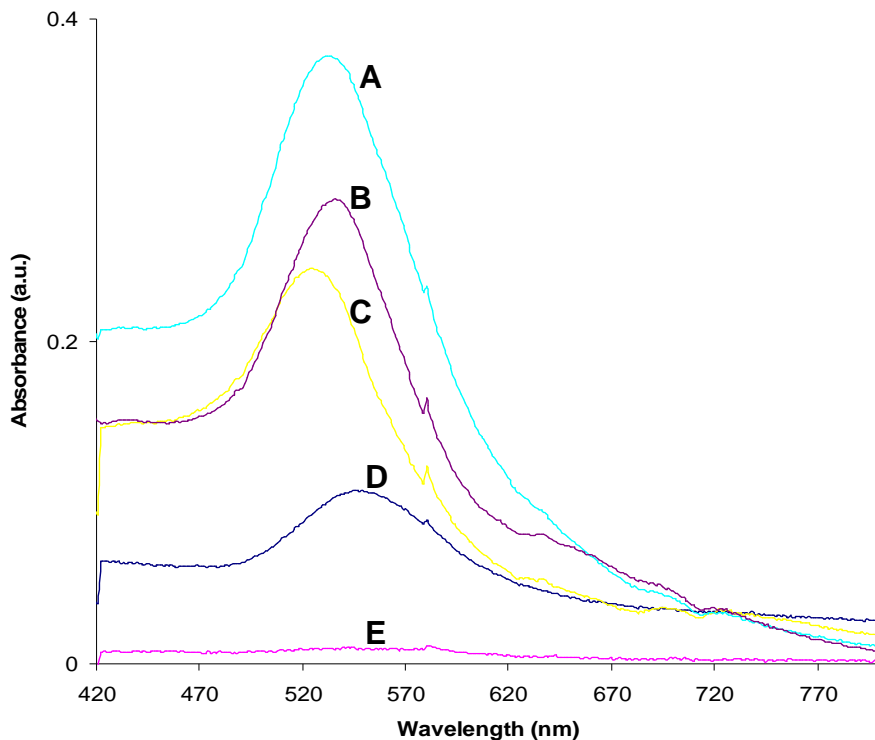


**Figure 3.14:** UV-Visible absorption spectra of AuNPs at various solvents and various irradiation times; (A) 5 hours in ethanol, (B) 5 hours in Acetonitrile, (C) 5 hours in water, (D) 5 minutes in water, and (E) 5 minutes in ethanol.

Figure 3.15 shows TEM images of AuNPs obtained in the three solvents (water, ethanol and acetonitrile). Water has been the primary solvent in which anisotropic nanomaterials are prepared. However, as seen in Figure 3.15B and C, ethanol can also produce well dispersed particles with varied shapes at room temperature. Over 90 % of nanoparticles produced in ethanol were non-spherical, different shapes including nanorods with an average length of 40 nm, were observed. The polarity of water molecules is stronger than that of ethanol molecules. Theoretically, the asymmetrical distribution of the charges on the particle surface can take place due to the coulombic interaction in both water and ethanol solutions. Liao *et al.* [25] have found that ethanol caused chain-like aggregation of AuNPs. The yield of the sample synthesized in acetonitrile was low with the particles close to spherical in shape.

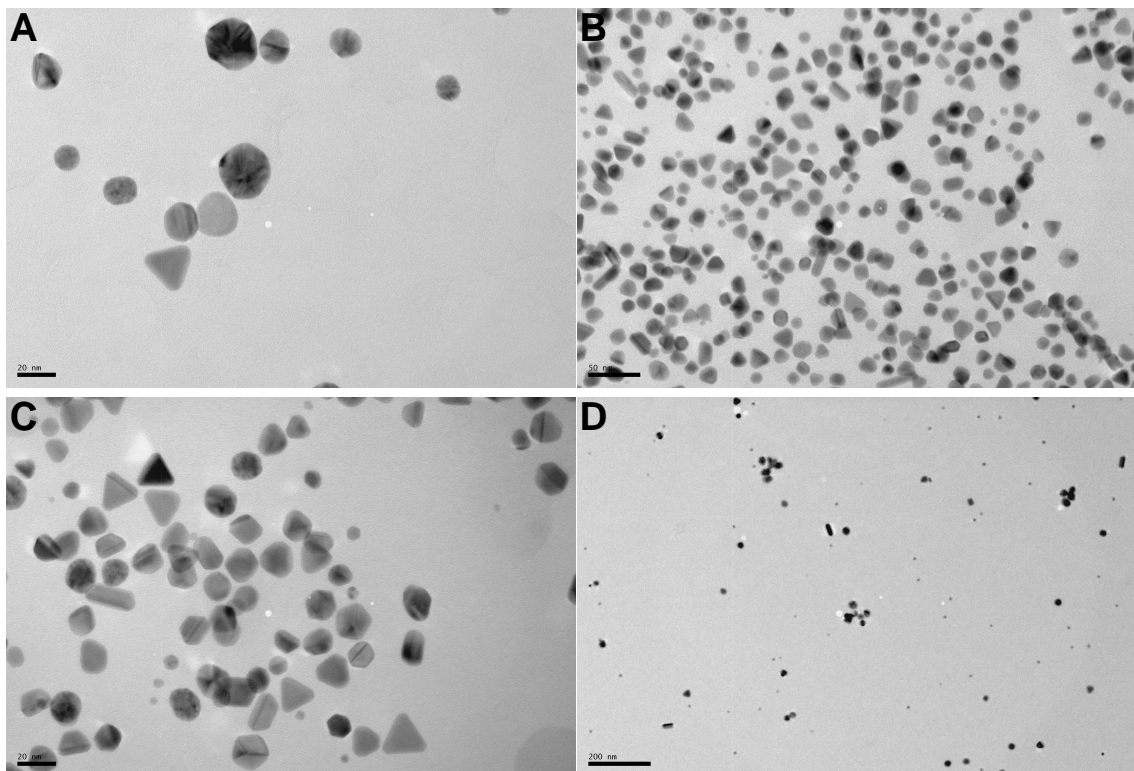


**Figure 3.15:** TEM images of AuNPs at different solvents for the samples taken at longest irradiation time (5 hours); (A) in water, (B and C) in ethanol, and (D) in acetonitrile.

### 3.2.5 Variation of Irradiation Time

The growth of gold nanoparticles was monitored with respect to time, i.e. exposure of the solution to UV light. Figure 3.16 displays the UV-Visible spectra of gold nanoparticles as exposure / irradiation time increases. The irradiation was varied from 5 minutes to 5 hours. From the spectrum at these time intervals it is clearly seen that at the shortest exposure time (5 minutes) nanoparticles are not present as no absorption is observed. As the exposure time increases a broad absorption peak is observed which sharpens at the longest irradiation time (5 hours). A blue shift in the absorption spectrum can be observed with an increase in the irradiation time. The nanoparticles at 1 h and below (except 5 min) exposure showed absorption at 545 nm. Above 1 h a blue shift is observed at different absorption plasmon i.e. 90 min (542 nm), 3 h (537 nm) and 5 h (535 nm). This blue shift towards 530 nm and sharp absorption peaks at longer irradiation times are a result of the formation of well dispersed and well defined gold nanoparticles.

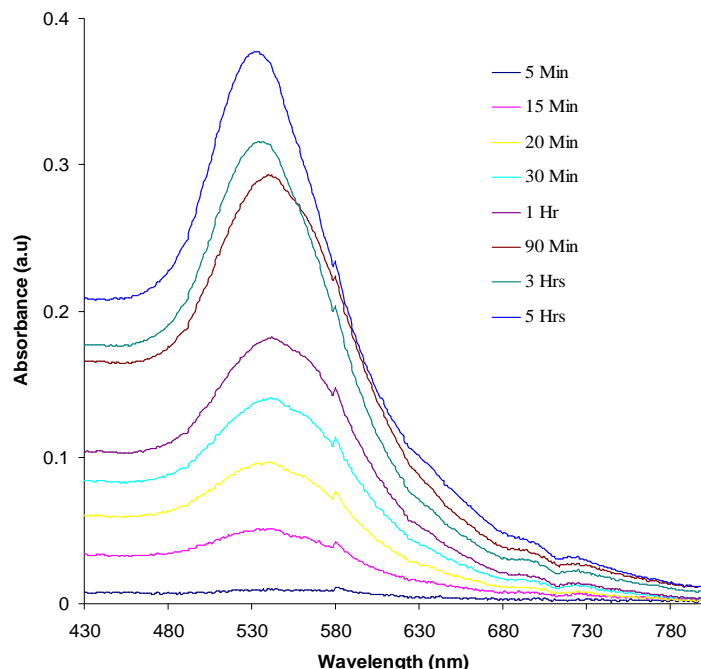


**Figure 3.16:** UV-Visible absorption spectra of AuNPs at various irradiation times.

### 3.2.6 Synthesis of Gold Nanoparticles in the Presence of Citric Acid

In this experiment, we report the simultaneous irradiation of a solution blended with the photosensitive agent (citric acid), the reactant precursor and the protective agent (PVP), as detailed in experiment 8 of Table 3.1. In the experiments reported earlier, the irradiation time has been found to be the most important parameter that had a strong influence on the size and shape of gold nanoparticles. Figure 3.17 shows the influence of the irradiation time on the plasmon absorption band of the produced gold nanoparticles in the presence of citric acid. It indicates that the intensity of the absorption band increases with increasing irradiation time. Absorption bands at shorter irradiation times are red-shifted to the normal gold absorption at 530 nm as they absorb at 532 nm (both 8 and 16 min), while those at longer irradiation time are slightly blue-shifted, i.e. 529 nm (30 min) and 527 nm (60 min) and are indicative of a decrease in particle diameter [26]. At shorter irradiation time, citric acid forms reduced radicals induced by ultraviolet radiation and possibly the reduction reaction of Au (III) to Au (I) also occurred. The reduction of Au (III) or Au (I) to Au (0) also occurs. As irradiation time is further increased the reaction becomes saturated with no further formation of nanoparticles.

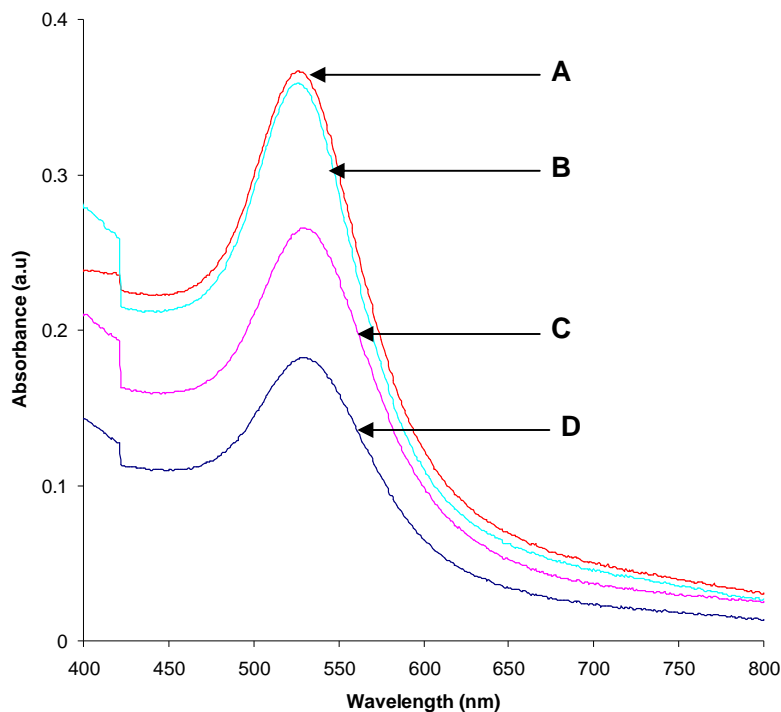


**Figure 3.17:** UV-Visible absorption spectra of AuNPs at various irradiation times in the presence of citric acid (A) 30 minutes, (B) 60 minutes, (C) 16 minutes, and (D) 8 minutes.

Yang *et al.* have shown that additives such as PVP can greatly decrease the particle size and narrow the size distribution with the continuous UV-irradiation method [17]. However, whether the photo reduction of Au (III), the growth process of gold nanoparticles and its size and shape are pH dependent is still questionable. In this particular experiment citric acid is used as a capping ligand for stabilizing the metal nanoparticles as well as the photo reduction agent for the metal ions. Au (III) ions are reduced to Au<sup>0</sup> by photo produced free radicals and negative electrons. Citric acid is known to form complexes with copper, iron and silver; and it is tetradentate in these complexes [27,28]. In this case, the Au (III) ions are partly complexed by citric acid [28], which then leads to the blue shift and even weakening of ligand to metal charge transfer (LMCT) band of AuCl<sub>4</sub><sup>-</sup>. It is well known that the optical properties of metal nanoparticles strongly depend on the size and shape of nanoparticles, especially for anisotropic gold nanoplates [29].

The TEM images (Figure 3.18) show predominantly spherical particles which show some degree of aggregation. Particles in the shape of truncated triangles, pentagons and rods are also present. The micrographs presented were taken at longest irradiation time (60 min). Figure 3.19 shows the HRTEM and SAED of the gold particles. The lattice fringes observed in the HRTEM images demonstrate that the particles are crystalline in nature. Figure 3.20 presents the results obtained from the XRD analysis. All the diffraction peaks can be indexed to the characteristic peaks of the fcc crystalline structure of gold. The peaks are assigned to the diffraction from the (111), (200), (220) and (311) planes of fcc gold, respectively (JCPDS File 04-0784).

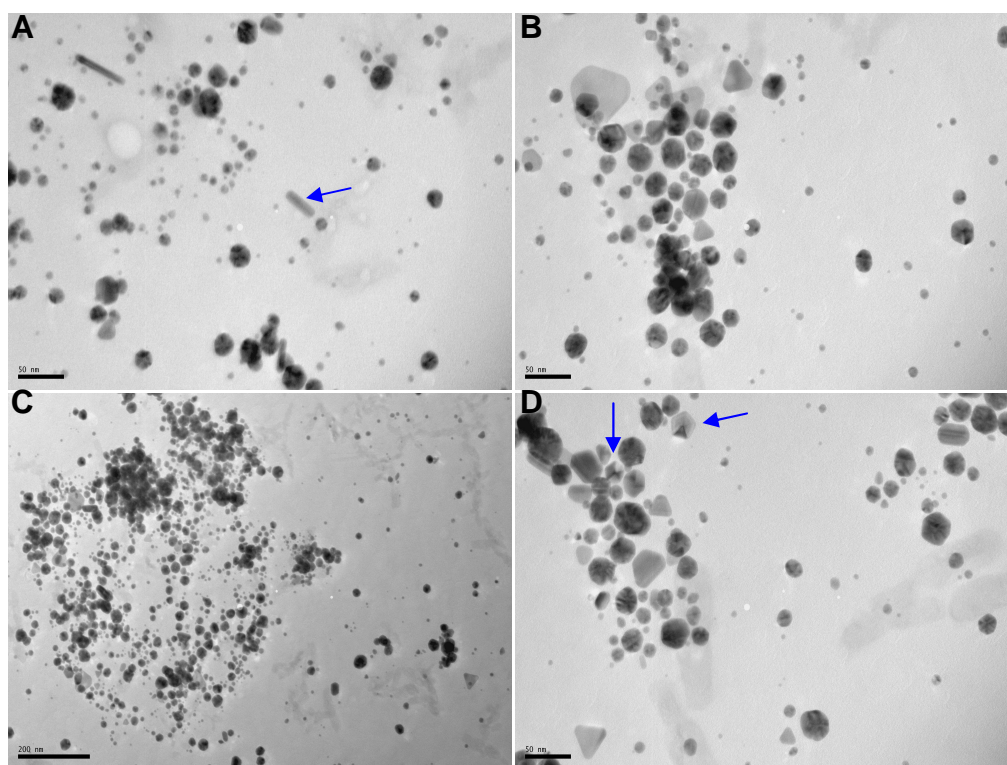


**Figure 3.18:** TEM images of AuNPs at different magnification for the samples taken at longest irradiation time (60 minutes) in the presence of citric acid.

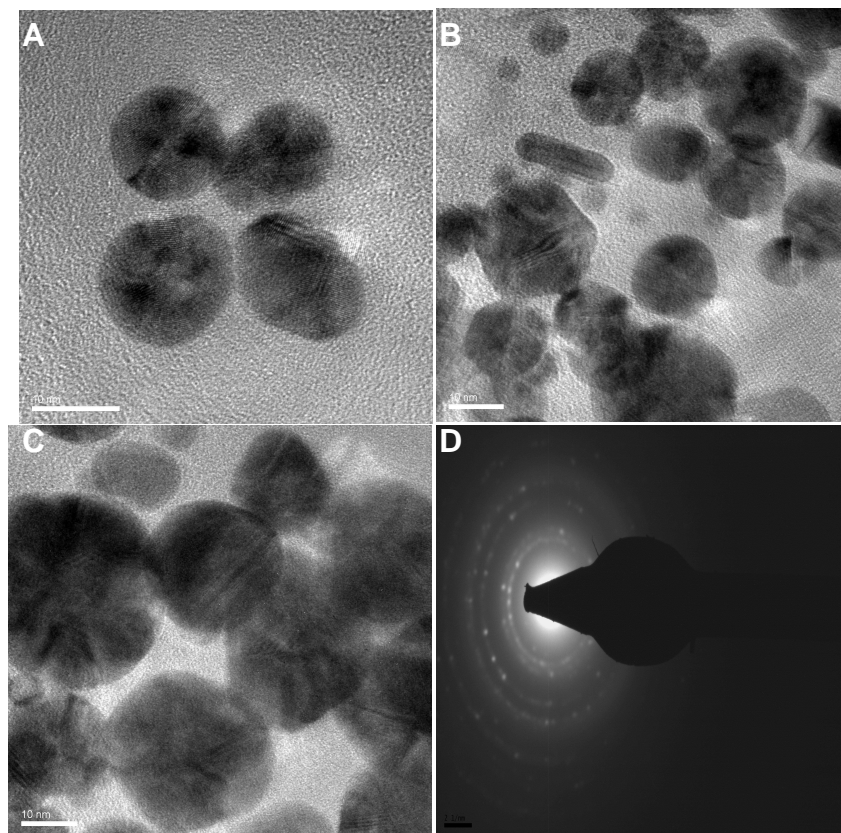


**Figure 3.19:** A, B and C are HRTEM images of AuNPs for the sample taken at longest irradiation time (60 minutes) in the presence of citric acid, D is the SAED pattern.

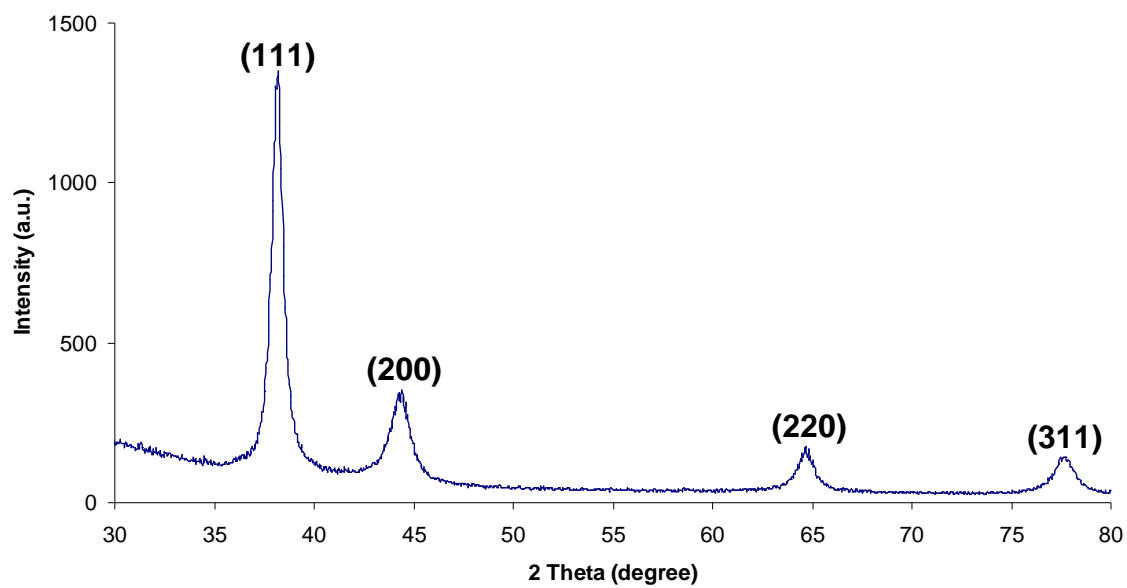


**Figure 3.20:** Powder XRD pattern of the AuNPs in the presence of citric acid.

### 3.3 CONCLUSIONS

Shape-controlled gold nanoparticles have been synthesized using an ultraviolet irradiation technique at room temperature. This is a simple route to synthesize anisotropic gold nanoparticles in the presence of water soluble polymer, PVP. It was found that not only the concentration of Au cations and the irradiation time but also the concentration and the species of the polymer capping materials, solvents and lamp wavelength all played important roles in the morphological control of the produced Au nanoparticles. Increasing  $\text{HAuCl}_4$  concentration and prolonging irradiation time facilitated the formation of AuNPs with regular shapes (i.e. triangular, truncated triangular, pentagon, hexagon, nanoprisms, rods, octahedral and decahedral were all observed). The particle size was found to be within the nanometer range for most of the experiments conducted. The precursor concentration variation showed the dominance of non-spherical AuNPs with average size ranging from 30 – 50 nm, and multiple-twinned particles were also observed when the precursor concentration was varied. The high resolution TEM clearly showed the lattice fringes that confirm the crystallinity of the formed AuNPs, which is also evident from XRD and SAED patterns. By varying the ratio between capping agent and precursor concentration in the initial solution, the kinetics of the reaction was manipulated and several morphologies were obtained including spherical polycrystalline nanoparticles and other non-spherical shapes (i.e. truncated triangular, pentagon, hexagon, nanoprisms, rods, octahedral and decahedral). The use of ethanol as the solvent resulted in the well-dispersed non-spherical AuNPs. Different plasmon absorption was observed with the varied irradiation time and a blue-shift was noted for increased irradiation time. The presence of citric acid resulted in the formation of crystalline AuNPs which is clear from the optical properties, TEM and their crystallographic studies.

The advantages of the process described above are that it is simple and efficient to achieve the uniform anisotropic AuNPs at room temperature and short reaction time of 5 minutes. PVP plays a crucial role to promote the nucleation and formation of Au nanoparticles and the size control was achieved by adjusting its concentration. This capping agent controlled the growth rate between the {100} and {111} plane directions by altering with their surface energies. At certain stages adsorption along the {111}

surface is probably favoured due to its low surface free energy resulting in the formation of {111} facets and decahedral multiply-twinned particles (MTPs). The formation of aggregated nanoplates was observed in the absence of PVP. In other reactions the presence of citric acid acted as a capping ligand for stabilizing the metal nanoparticles as well as a photoreduction agent for the metal ions. Most of the AuNPs produced were dominated by truncated triangular nanoparticles whose edge length varied from 30 – 60 nm. These structures may possess interesting new collective physical properties that are different from those of the original bulk material and are expected to be applicable as building blocks in constructing devices in future nanoelectronics. In chapter 4 the synthesis of CdSe and gold-CdSe hybrid nanoparticles using different methods is discussed.

**3.4 REFERENCES**

- 
- [1] Y. Sun, Y. Xia, *Science*, 2002, **298**, 2176.
- [2] D.J. Milliron, S.M. Highes, Y. Cui, L. Manna, J. Li, L. Wang, A.P. Alivisatos, *Nature*, 2004, **430**, 190.
- [3] T.S. Ahmadi, Z.L. Wang, T.C. Green, A. Henglein, M.A. El-Sayed, *Science*, 1996, **272**, 1924.
- [4] R. Jin, Y. Cao, G.S. Metraux, G.C. Schartz, C.A. Mirkin, *Nature*, 2003, **425**, 487.
- [5] X.C. Jiang, A. Brioude, M.P. Pileni, *Colloids Surf. A, Physicochem. Eng. Asp.*, 2005, **257**, 161.
- [6] J.L. Burt, J.L. Elechiguerra, J. Reyes-Gasga, J.M. Montejano-Carrizales, M.J. Jose-Yacaman, *Cryst. Growth*, 2005, **285**, 681.
- [7] Y. Yin, R.M. Rioux, C.K. Erdonmez, S. Hughes, G.A. Somorjai, A.P. Alivisatos, *Science*, 2004, **304**, 711.
- [8] M.A. El-Sayed, *Acc. Chem. Res.*, 2001, **34**, 257.
- [9] R.C. Jin, Y.W. Cao, C.A. Mirkin, K.L. Kelly, G.C. Schartz, J.G. Zheng, *Science*, 2001, **294**, 668.
- [10] A. Henglein, D. Meisel, *Langmuir*, 1998, **14**, 7392.
- [11] E. Hao, G. Schartz, J. Hupp, *J. Fluoresc.*, 2004, **14**, 331.
- [12] K.L. Kelly, E. Coronado, L.L. Zhao, G.C. Schartz, *J. Phys. Chem. B*, 2003, **107**, 668.
- [13] O.R. Miranda, T.S. Ahmadi, *J. Phys. Chem. B*, 2005, **109**, 15724.
- [14] S. Yang, Y. Wang, Q. Wang, R. Zhang, B. Ding, *Colloids Surf. A Physicochem. Eng. Asp.*, 2007, **296**, 37.
- [15] Y. Chen, X. Gu, C.G. Nie, Z.Y. Jiang, Z.X. Xie, C.J. Lin, *Chem. Commun.*, 2005, **5**, 4181.
- [16] W.R. Meson, H.B. Gray, *Inorg. Chem.*, 1968, **7**, 55.
- [17] S.C. Yang, T.W. Zhang, L. Zhang, S.X. Wang, Z.M. Yang, B.J. Ding, *Colloid Surf. A*, 2006, **296**, 37.
- [18] B. Wiley, Y. Sun, J. Chen, H. Cang, Z.Y. Li, X. Li, Y. Xia, *MRS Bulletin*, 2005, Vol. 30.

- 
- [19] Y. Sun, B. Mayers, T. Herricks, Y. Xia, *Nano Lett.*, 2003, **3**, 955.
- [20] Y. Sun, B. Gates, B. Mayers, Y. Xia, *Nano Lett.*, 2002, **2**, 165.
- [21] A. Guinier, *X-Ray Diffraction*, W.H. Freeman: San Francisco CA, 1963.
- [22] J. W. Mullin, *Crystallization*, 3<sup>rd</sup> ed., Oxford, 1997.
- [23] M.J. Yacaman, J.A. Ascencio, H.B. Liu, J. Gardea-Torresdey, *J. Vac. Sci. Technol. B*, 2001, **19**, 1091.
- [24] L. Marks, *Rep. Prog. Phys.*, 1994, **57**, 603.
- [25] J. Liao, Y. Zhang, W. Yu, L. Xu, *Colloids and Surfaces A: Physicochem. Eng. Aspects*, 2003, **223**, 177.
- [26] P.V. Kamat, *J. Phys. Chem. B*, 2002, **106**, 7729.
- [27] A. Henglein, M. Giersig, *J. Phys. Chem. B*, 1999, **103**, 9533.
- [28] T. John, P.C. Stevenson, J. Hillier, *J. Discuss, Faraday Soc.*, 1951, **11**, 55.
- [29] B. Liu, J. Xie, J.Y Lee, Y.P. Ting, J.P. Chen, *J. Phys. Chem. B*, 2005, **109**, 15256.